IJCRT.ORG ISSN : 2320-2882

INTERNATIONAL JOURNAL OF CREATIVE RESEARCH THOUGHTS (IJCRT)

An International Open Access, Peer-reviewed, Refereed Journal

Formulation And Characterization Of Folate Conjugated Peg Spacer-Based Nanoparticle For The Effective Targeting Against Breast Cancer Cell Line

Sailesh Chandra Biswal[1], Dr. Arun Patel[*]

Shri Ram Group of Institutions, Faculty of Pharmacy, Jabalpur – 482002, (M.P.)

Abstract

Conventional chemotherapy is frequently hampered by a lack of tumor selectivity, resulting in systemic toxicity and a narrow therapeutic window. To address these limitations, this study reports the design, synthesis, and evaluation of actively targeted solid lipid nanoparticles (SLNs) for the enhanced delivery of paclitaxel (PTX). A series of PTX-loaded SLNs were developed and surface-functionalized with folic acid (FA) as a targeting ligand. The formulations included SLNs with FA conjugated directly to the surface (SLNFA) and SLNs with FA attached via polyethylene glycol (PEG) spacers of two different molecular weights, 1000 Da (SLNP1FA) and 4000 Da (SLNP4FA). Physicochemical characterization revealed that surface modification progressively increased particle size while maintaining a narrow distribution, and significantly enhanced drug entrapment. The SLNP4FA formulation demonstrated the highest drug entrapment efficiency at 58.22% and exhibited the most sustained in vitro drug release profile over 48 hours. The therapeutic efficacy of the nanocarriers was assessed against folate receptor (FR)-positive MCF-7 human breast cancer cells. All folate-targeted formulations showed superior cytotoxicity compared to free PTX and non-targeted SLNs. Crucially, the efficacy was dependent on the PEG spacer length, with SLNP4FA exhibiting the highest potency. This formulation achieved an IC50 value of 331.29 nM, representing a 48.39% reduction in the IC50 compared to free PTX. These findings demonstrate that optimizing the PEG spacer length is a critical strategy for overcoming steric hindrance and maximizing receptor-mediated endocytosis.

The FA-PEG (4000)-SLN architecture represents a highly effective and promising platform for the targeted delivery of chemotherapeutic agents to solid tumors.

Key Words- *solid lipid nanoparticles; paclitaxel; nanocarriers; breast cancer.*

1. Introduction

Cancer remains a primary cause of mortality worldwide, and despite significant advances, the efficacy of conventional chemotherapy is often constrained by profound limitations. Most traditional anticancer agents, such as paclitaxel, exhibit a narrow therapeutic window, a consequence of their inability to discriminate between malignant and healthy tissues. This lack of selectivity leads to dose-limiting systemic toxicity and severe adverse effects, which compromise patient quality of life and can necessitate the cessation of treatment. Furthermore, the complex microenvironment of solid tumors presents a formidable set of physiological barriers that impede drug delivery. These include elevated interstitial fluid pressure, a chaotic and leaky vasculature, and a dense extracellular matrix, all of which hinder the penetration and accumulation of therapeutic agents at the target site.

In response to these challenges, the field of cancer nanotechnology has emerged, offering a revolutionary paradigm for cancer therapy. Nanoparticulate drug delivery systems, typically ranging from 10 to 500 nm in size, possess unique properties that enable them to overcome the limitations of conventional drugs. These nanosystems can be engineered to carry a large therapeutic payload, protect the encapsulated drug from premature degradation, bypass traditional drug resistance mechanisms, and facilitate targeted delivery. A foundational principle governing the behavior of nanoparticles in oncology is the Enhanced Permeability and Retention (EPR) effect. Tumors are characterized by aberrant angiogenesis, resulting in blood vessels with poorly sealed endothelial junctions and a discontinuous basement membrane. This "leaky" vasculature permits the extravasation of nanoparticles into the tumor interstitium. Concurrently, tumors exhibit functionally defective lymphatic drainage, which prevents the clearance of these accumulated nanoparticles, leading to their passive retention and concentration within the tumor mass.

Among the various nanocarriers available, Solid Lipid Nanoparticles (SLNs) have garnered significant attention as a promising platform for anticancer drug delivery. SLNs are colloidal carriers composed of a solid lipid core stabilized by surfactants. Their primary advantage lies in their composition from physiological and biodegradable lipids, which minimizes the risk of acute and chronic toxicity. They combine the benefits of other systems, such as the structural stability of polymeric nanoparticles and the biocompatibility of liposomes, while avoiding drawbacks like the use of organic solvents in some preparations and potential immunogenicity. The solid matrix of SLNs also provides an excellent environment for the controlled and sustained release of encapsulated lipophilic drugs.

While the EPR effect provides a basis for passive tumor targeting, the therapeutic index can be further improved through active targeting strategies. This approach involves functionalizing the nanoparticle surface with ligands that bind to specific receptors overexpressed on cancer cells. The folate receptor (FR) is an exemplary target for this strategy. The FR is a high-affinity cell surface receptor for the vitamin folic acid (FA) and is significantly overexpressed in a wide array of human cancers, including those of the breast, ovary, lung, and brain, while its expression in most normal tissues is minimal. FA is an ideal targeting ligand due to its small size, high stability, non-immunogenicity, and straightforward conjugation chemistry, making it a powerful tool for directing nanocarriers specifically to tumor cells.

A critical, yet often overlooked, aspect of designing targeted nanocarriers is the interplay between the targeting ligand and other surface modifications, particularly polyethylene glycol (PEG). PEGylation is a widely adopted strategy to create "stealth" nanoparticles that can evade recognition by the reticuloendothelial system (RES), thereby prolonging their circulation time and enhancing their accumulation in tumors via the EPR effect. However, this protective PEG layer can also create a steric barrier that physically hinders the interaction between the targeting ligand (FA) and its cognate receptor on the cell surface. This presents a fundamental design conflict: the need for a stealth coating for long circulation is often at odds with the need for an accessible ligand for active targeting. A sophisticated engineering solution to this problem is the use of a PEG chain as a flexible "spacer" or "linker" that extends the targeting ligand away from the nanoparticle surface, projecting it beyond the steric shield of the main PEG coating. The length of this spacer is hypothesized to be a critical design parameter. A spacer that is too short may fail to overcome the steric hindrance, while an excessively long one might introduce other undesirable complexities. This study was therefore designed to systematically investigate this hypothesis by developing a series of paclitaxel-loaded SLNs where folic acid is either conjugated directly or tethered via PEG spacers of 1000 Da and 4000 Da. By comparing the physicochemical properties and in vitro anti-tumor efficacy of these distinct nanoarchitectures, this work aims to elucidate the role of spacer chain length in optimizing receptor-mediated targeting and to identify the most effective design for folate-targeted cancer therapy.

2. Materials and Methods

2.1. Materials

Paclitaxel (PTX) was received as a gift sample from SUN Pharmaceutical Industries Ltd, Gujarat, India. Soya Phosphatidyl Choline (SPC) was procured from Himedia. Tristearin, stearylamine, Tween 80, Folic Acid (FA), Polyethylene Glycol (PEG) with molecular weights of 1000 Da and 4000 Da, 1-Ethyl-3-[3-dimethylaminopropyl] carbodiimide (EDC), N-hydroxysuccinimide (NHS), 1,1'-Carbonyldiimidazole (CDI), N,N'-Dicyclohexylcarbodiimide (DCC), and 4-(Dimethylamino)pyridine (DMAP) were of analytical grade and purchased from local vendors. For cell culture studies, Dulbecco's Modified Eagle Medium (DMEM), Fetal Bovine Serum (FBS), and 3-(4,5-dimethylthiazol-2-yl)-2,5-diphenyltetrazolium bromide (MTT) were

used. The MCF-7 human breast cancer cell line was utilized for all ex vivo experiments. Deionized water was used throughout all experiments.

2.2. Preformulation Studies of Paclitaxel

The identity and physicochemical properties of the bulk PTX drug were confirmed prior to formulation. The drug appeared as a white to off-white crystalline powder. The melting point was determined using a standard melting point apparatus and was found to be in the range of 216-217°C. The solubility of PTX was qualitatively assessed in various solvents, revealing it to be practically insoluble in water and phosphate-buffered saline (PBS, pH 7.4), but freely soluble in ethanol, chloroform, and dimethyl sulfoxide (DMSO). The absorption maximum (λmax) was determined by scanning a solution of PTX in a methanol:PBS (30:70) mixture from 200-400 nm using a UV/Visible spectrophotometer (Shimadzu 1800, Japan), and was found to be 237.0 nm. The partition coefficient (Po/w) was determined in n-octanol/water and n-octanol/PBS (pH 7.4) systems and was calculated to be 3.50 and 3.59, respectively, confirming the lipophilic nature of the drug.

2.3. Preparation of Paclitaxel-Loaded SLNs

PTX-loaded SLNs were prepared using a solvent injection method. A lipid phase was prepared by dissolving Tristearin, SPC, stearylamine, and 10 mg of PTX in a minimal amount of absolute ethanol. This organic solution was heated to 70°C in a beaker. Concurrently, an aqueous phase was prepared by dissolving Tween 80 (0.5% v/v) in distilled water and heating it to the same temperature (70°C). The hot organic phase was then rapidly injected into the hot aqueous phase under constant magnetic stirring. The resulting pre-emulsion was immediately subjected to high-intensity sonication using a probe sonicator to form a homogenous dispersion of SLNs.

2.4. Synthesis of Folate-Conjugated Nanocarriers

2.4.1. Direct Conjugation (SLNFA)

The synthesis of SLNFA was performed in two steps. First, the active NHS ester of FA was prepared. FA (0.064 mmol) was dissolved in DMSO (10.0 mL), to which NHS (0.064 mmol) and EDC (0.064 mmol) were added. The solution was stirred for 24 hours at room temperature in the dark. The active ester of FA was precipitated with acetone, collected by filtration, and dried under vacuum. In the second step, the prepared active ester of FA was dissolved in DMSO and added to a solution of amine-terminated SLNs (0.01 mmol) in DMSO. The mixture was stirred for 2 days at room temperature. The resulting SLNFA nanoconjugate was precipitated with acetone, collected, and purified using a Sephadex G-50 column with DMSO as the eluent.

2.4.2. Indirect Conjugation via PEG Spacers (SLNP1FA and SLNP4FA)

The synthesis of PEG-spacer-linked nanoconjugates involved a three-step process.

Step 1: Activation of PEGs. PEGs (Mw 1000 and 4000 Da, 0.064 mmol each) were separately dissolved in DMSO (5.0 mL), and CDI (0.064 mmol) was added. Each mixture was stirred for 1 hour at room temperature to yield CDI-activated PEGs. **Step 2: Preparation of SLN-PEG intermediates.** The CDI-activated PEGs were added to amine-terminated SLNs (0.01 mmol) in DMSO and stirred for 2 days. The resulting SLN-PEG conjugates were precipitated with acetone and purified over a Sephadex G-50 column. **Step 3: Conjugation of FA to SLN-PEG intermediates.** FA (0.064 mmol) was dissolved in DMSO, and DCC (0.064 mmol) and DMAP (0.064 mmol) were added and stirred for 2 hours. The SLN-PEG intermediates were then added to this reaction mixture and stirred for an additional 12 hours under a nitrogen atmosphere. The final SLN-spacer-FA nanoconjugates (SLNP1FA and SLNP4FA) were precipitated with acetone, collected, and purified using a Sephadex G-50 column.

2.5. Physicochemical and Spectroscopic Characterization

2.5.1. Spectroscopic Confirmation

The successful synthesis of all nanoconjugates was confirmed using Fourier-Transform Infrared (FT-IR) spectroscopy and Proton Nuclear Magnetic Resonance (1H NMR) spectroscopy. FT-IR spectra were recorded using a Nujol mull method. 1H NMR spectra were obtained on a 300 MHz spectrometer using D$_2$O as the solvent.

2.5.2. Particle Size, Polydispersity Index (PDI), and Zeta Potential

The average particle size, PDI, and zeta potential of the nanocarriers were measured using a Zetasizer (Malvern Instrument, UK) based on photon correlation spectroscopy. Samples were appropriately diluted with deionized water before analysis.

2.5.3. Morphological Analysis

The shape and surface morphology of the nanoparticles were visualized using a Transmission Electron Microscope (TEM) (Philips Morgagni 268). A drop of the diluted nanoparticle dispersion was placed on a formvar-coated copper grid, negatively stained with uranyl acetate, and observed at an acceleration voltage of 100 kV.

2.6. Drug Entrapment Efficiency and In Vitro Release Studies

2.6.1. Entrapment Efficiency

The entrapment efficiency of PTX was determined using a Sephadex G-50 minicolumn centrifugation method to separate the free drug from the SLNs. A 0.2 mL aliquot of the SLN dispersion was applied to the column and centrifuged at 2000 rpm for 2 minutes. The eluted fraction containing the SLNs was collected and lysed

with 0.01% Triton-X100 to release the entrapped drug. The concentration of PTX was then quantified spectrophotometrically at 237 nm. The entrapment efficiency was calculated as the ratio of the amount of entrapped drug to the total initial amount of drug used.

2.6.2. In Vitro Drug Release

The in vitro release of PTX from the various nanoformulations was studied using a dialysis bag method. A 5 mL sample of the purified SLN dispersion was placed in a dialysis bag (MWCO 10,000 Da). The bag was immersed in 100 mL of PBS (pH 7.4) maintained at 37°C with continuous magnetic stirring. At predetermined time intervals, aliquots were withdrawn from the release medium and replaced with an equal volume of fresh PBS to maintain sink conditions. The concentration of PTX in the withdrawn samples was determined spectrophotometrically at 237 nm.

2.7. Ex Vivo Antitumor Studies

2.7.1. Cell Culture

The MCF-7 human breast cancer cell line, which overexpresses the folate receptor, was used for cytotoxicity and uptake studies. The cells were cultured in DMEM supplemented with 10% FBS and 1% penicillin-streptomycin mixture. Cultures were maintained in a humidified incubator at 37°C with 5% CO$_2$.

2.7.2. MTT Cytotoxicity Assay

The cytotoxic activity of the formulations was evaluated using the MTT assay. MCF-7 cells were seeded in 96-well plates at a density of 5×103 cells/well and incubated for 24 hours. The cells were then treated with various concentrations (50-1600 nM) of free PTX, plain SLNs, SLNFA, SLNP1FA, and SLNP4FA for 48 hours. After the treatment period, 10 µL of MTT reagent (5 mg/mL) was added to each well, and the plates were incubated for an additional 2 hours. Subsequently, 100 µL of a lysing buffer was added to dissolve the formazan crystals. The optical density (OD) was measured at 570 nm using a microplate reader. The percentage of cell viability was calculated using the formula: % Cell Viability = (ODsample/ODcontrol)×100. The half-maximal inhibitory concentration (IC50) was determined from the dose-response curves.

2.7.3. Cellular Uptake Study

The cellular uptake and morphological effects of the formulations were qualitatively assessed by microscopy. MCF-7 cells were seeded in a 6-well plate at a density of 5×103 cells/well. After 24 hours, the cells were treated with the different formulations. After a 48-hour incubation period, the cells were observed under an inverted microscope (Leica, Germany) to assess changes in cell count, colony formation, and morphology indicative of cytotoxicity and uptake.

2.8. Statistical Analysis

All quantitative data were expressed as mean ± standard deviation (SD) from at least three independent experiments. Statistical analysis was performed using GraphPad Instat Software. Comparisons between groups were made using either an unpaired t-test or a one-way analysis of variance (ANOVA) followed by the Tukey-Kramer multiple comparison test. A p-value of less than 0.05 was considered statistically significant.

3. Results and Discussion

3.1. Synthesis and Structural Confirmation of Nanoconjugates

The successful synthesis of the folate-targeted nanoconjugates was predicated on a series of well-defined chemical reactions to covalently link the targeting moieties to the surface of the amine-terminated SLNs. The formation of these linkages was rigorously confirmed using spectroscopic techniques. The FT-IR spectrum of the directly conjugated SLNFA formulation displayed characteristic peaks that were absent in the precursor SLNs. Notably, the appearance of a peak corresponding to aromatic C=C bending and stretching at 1673.75 cm^{-1} and an aromatic C-H bending peak at 789.83 cm^{-1} were indicative of the successful attachment of the pteridine ring system of folic acid. Furthermore, a new peak at 1416.11 cm^{-1} was assigned to the CH-NH-C(=O) amide bending vibration, confirming the formation of a stable amide bond between the carboxylic acid group of FA and the primary amine on the SLN surface. Similarly, the spectra for the PEG-spacer linked conjugates, SLNP1FA and SLNP4FA, showed the characteristic strong C-O stretching of the ether linkages within the PEG backbone (1114.71 cm^{-1} for SLNP1FA and 1107.21 cm^{-1} for SLNP4FA), along with the amide and aromatic peaks from the terminal FA, confirming the complete synthesis of the FA-PEG-SLN architecture. 1H NMR spectroscopy provided further, definitive evidence of successful conjugation. The spectrum for SLNFA showed new signals in the aromatic region, specifically at a chemical shift (δ) of 6.6 ppm, corresponding to the aromatic protons of the FA molecule. For the spacer-linked conjugates, SLNP1FA and SLNP4FA, the spectra were dominated by a large signal around 3.7-4.0 ppm, characteristic of the repeating methylene protons (-CH$_2$-CH$_2$-O-) of the PEG backbone. Critically, the appearance of signals corresponding to the aromatic protons of FA (e.g., δ = 6.6 ppm for SLNP1FA) and protons adjacent to the newly formed amide and ester bonds confirmed the covalent attachment of all components in the intended sequence. Collectively, these spectroscopic data provide unambiguous validation of the synthetic protocols and confirm the distinct surface chemistry of each of the prepared nanocarrier formulations.

3.2. Physicochemical Properties and Morphological Analysis

The physicochemical properties of the prepared nanoformulations are summarized in Table 1. The base PTX-loaded SLNs exhibited a mean particle size of 201.1 nm with a low polydispersity index (PDI) of 0.224, indicating a homogenous and monodisperse population of nanoparticles. As hypothesized, each subsequent surface modification step resulted in a systematic and significant increase in the hydrodynamic diameter. Direct conjugation of FA to form SLNFA increased the size to 249.4 nm. The introduction of the PEG spacers led to further increases, with SLNP1FA and SLNP4FA measuring 293.4 nm and 315.0 nm, respectively. This incremental increase in size serves as strong physical evidence corroborating the spectroscopic data, confirming the successful layering of the FA and FA-PEG moieties onto the SLN surface. Despite these increases, all formulations remained well within the 10-500 nm size range, which is considered optimal for leveraging the EPR effect for passive tumor accumulation. TEM analysis confirmed that all nanoparticles were spherical in shape and nanometric in size, consistent with the dynamic light scattering data.

A particularly noteworthy finding was the effect of surface modification on drug entrapment efficiency. As detailed in Table 1, the plain SLNs entrapped 31.09% of the initial PTX. Surface functionalization led to a marked increase in this value. The entrapment efficiency rose to 48.01% for SLNFA, 52.98% for SLNP1FA, and reached a maximum of 58.22% for SLNP4FA. This trend reveals a crucial aspect of the nanocarrier design that extends beyond simple surface targeting. The addition of the PEG corona fundamentally alters the drug-loading capacity of the nanoparticle. While the lipophilic PTX is primarily encapsulated within the solid lipid core, the hydrophilic, hydrated PEG layer on the surface appears to create an additional microenvironment capable of associating with or entrapping drug molecules. This phenomenon can be conceptualized as the PEG layer acting as a "drug sponge," providing additional space and interaction sites for the drug at the nanoparticle's periphery. The capacity of this "sponge" correlates directly with the length of the PEG chain; the larger PEG 4000 corona in SLNP4FA provides a more extensive and complex architecture for drug interaction, thereby resulting in the highest overall payload. This dual-compartment loading mechanism—a lipid core and a hydrophilic corona—is a significant finding, as it suggests that PEGylation can simultaneously enhance drug loading and provide stealth characteristics, making it a doubly advantageous strategy for drug delivery system design.

Table 1: Physicochemical Properties and Drug Entrapment of Prepared Nanocarriers.

Formulation Code	Size (nm ± SD)	Polydispersity Index (PDI)	% Drug Entrapped (± SD)
Plain SLNs	201.1 ± 3.7	0.224	31.09 ± 0.71
SLNFA	249.4 ± 2.6	0.238	48.01 ± 0.92
SLNP1FA	293.4 ± 3.4	0.325	52.98 ± 0.33
SLNP4FA	315.0 ± 3.4	0.395	58.22 ± 0.51

Data represent mean ± SD (n=3). Data compiled from.

Table 2: Solubility of PTX in different solvents

S. No.	Solvent	Solubility
1.	Distilled Water	-
2.	PBS (pH 7.4)	-
3.	Ethanol	++++
4.	Chloroform	++++
5.	Diethyl ether	++
6.	Dimethyl sulfoxide (DMSO)	++++

++++ Freely soluble 1-10 parts,
+++ Sparingly soluble 30-100 parts,
++ Soluble 30-100 parts,
+ Slightly soluble 100-1000 parts,
– Practically insoluble >10000 parts

Table 3: Partition coefficient values of PTX

S. No.	Solvent system	Partition Coefficient
1.	n-Octanol/Distilled water	3.50
2.	n-Octanol/PBS (pH 7.4)	3.59

Table 4: Important band frequencies in IR spectrum of PTX

S. No.	Wave No.(cm^{-1})	Description
1.	3509.8	OH stretching
2.	3245.7	NH stretching
3.	3019.0	=CH Stretching (Aromatic)
4.	1737.6	C=O Stretching
5.	1645.33	C=O Amide

Table 5: Standard Curve of PTX in Phosphate Buffer Solution (pH 7.4) at λ_{max} 237.0 nm

S.No.	Drug Conc. (µg/ml)	Absorbance	Regressed Absorbance	Statistical Parameters
1.	2	0.0990	0.1116	
2.	4	0.1594	0.1706	
3.	6	0.1982	0.2269	
4.	8	0.2659	0.2886	y = 0.033x + 0.011
5.	10	0.3419	0.3476	R^2 = 0.997
6.	12	0.4187	0.4066	
7.	14	0.4814	0.4656	
8.	16	0.5486	0.5246	
9.	18	0.6137	0.5836	
10.	20	0.6845	0.6625	

Table 6: Compatibility testing of drug with ingredient lipids

S. No.	Composition	Absorption maxima λmax (nm)	Absorbance
1.	PTX	237	0.5146
2.	PTX + SPC	237	0.5069
3.	PTX + Tristearin	237	0.4889

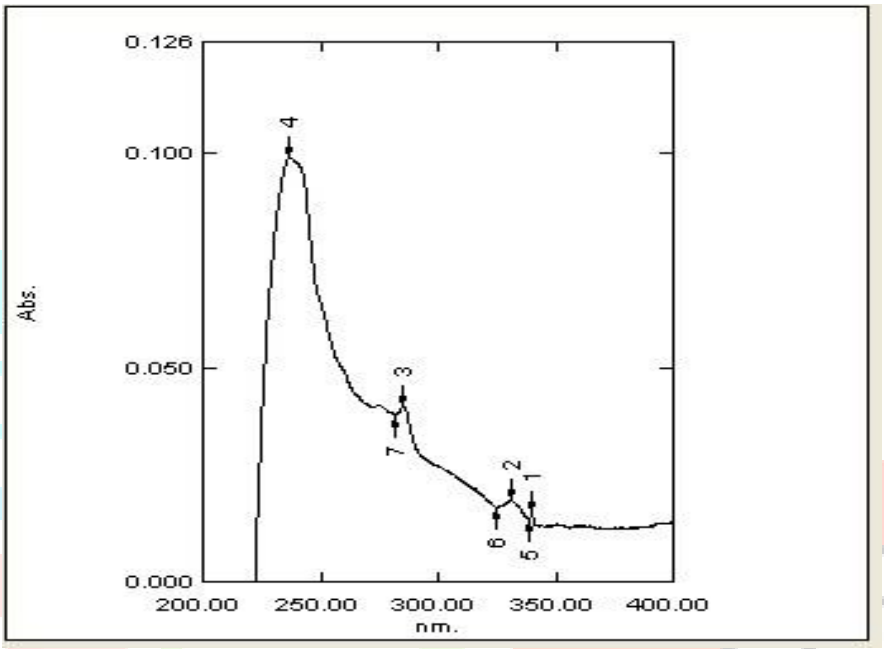

Figure 1: Absorption maxima of PTX Sample

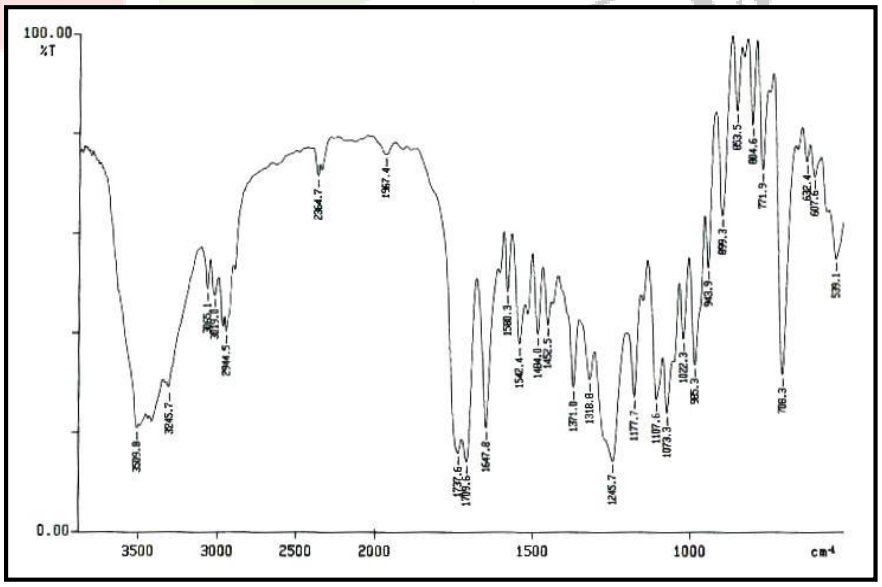

Figure 2: IR spectra of PTX (Sample)

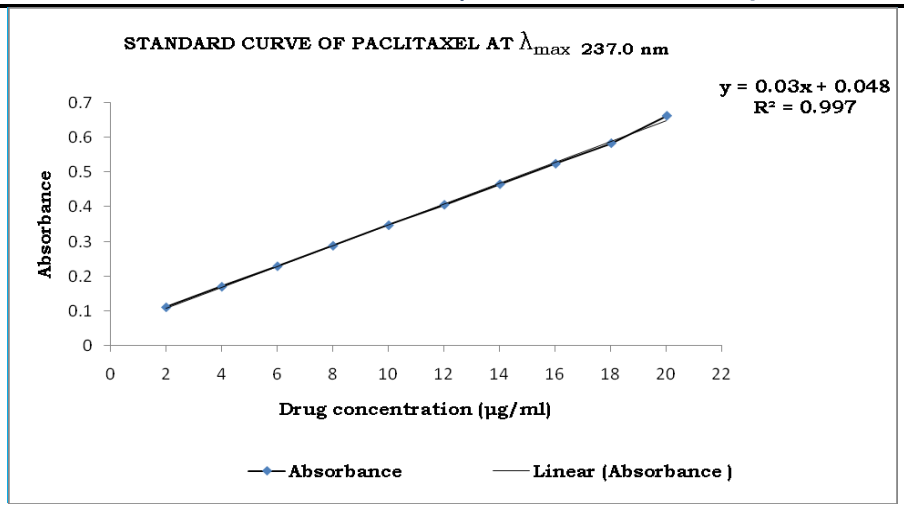

Figure 3: Linearly regressed standard curve of PTX in phosphate buffer solution (pH 7.4) at λ_{max} 237.0 nm

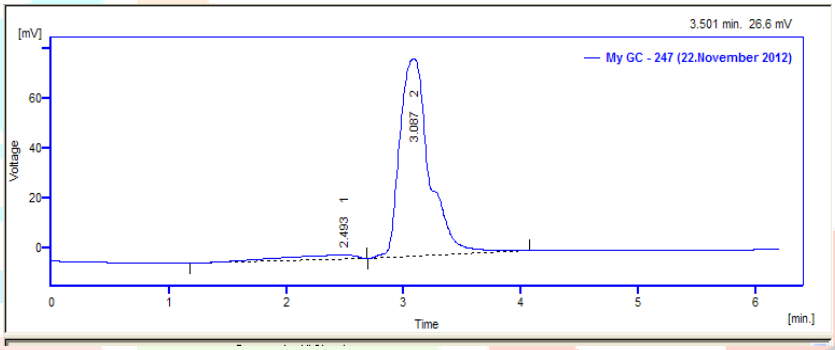

Figure 4: HPLC analysis of PTX

Table 7: Particle Size, PDI, % Drug Entrapment

Formulation Code	Size	Polydispersity Index	% Drug Entrapped
Plain SLNs	201.1 ± 3.7	0.224	31.09±0.71
Folate coupled SLNs SLNFA	249.4 ± 2.6	0.238	48.01±0.92
SLNP1FA	293.4± 3.4	0.325	52.98±0.33
SLNP4FA	315.0± 3.4	0.395	58.22±0.51

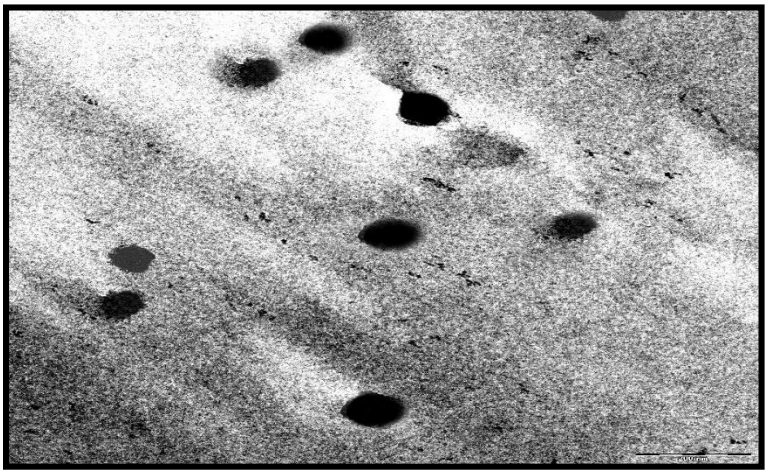

Figure 5: TEM image of plain SLNs

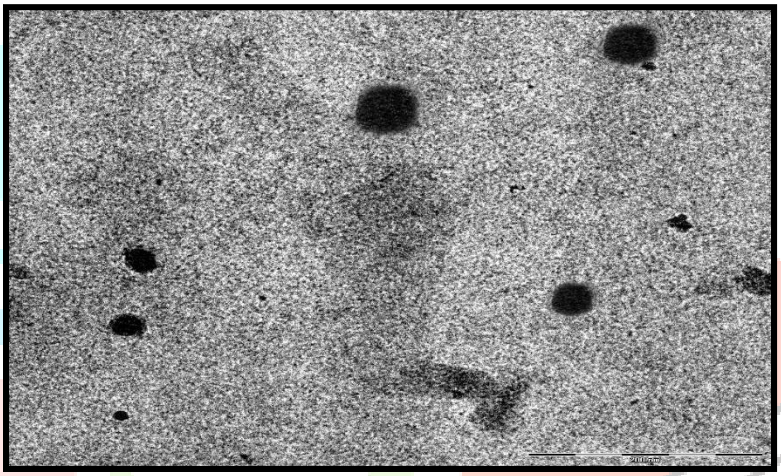

Figure 6: TEM image of coupled SLNs

3.3. In Vitro Paclitaxel Release Kinetics

The in vitro release of PTX from the different nanoformulations was monitored over 48 hours in PBS (pH 7.4) to simulate physiological conditions. All SLN-based formulations displayed a sustained release profile, characterized by an initial burst release followed by a slower, continuous release phase. This pattern is desirable for therapeutic applications, as it can help maintain drug concentrations within the therapeutic window for an extended period while minimizing toxic peaks. The surface modifications had a profound impact on the release kinetics. The plain SLN formulation exhibited the fastest release, with approximately 79.9% of the drug released after 48 hours. The conjugation of FA (SLNFA) slightly retarded the release, with a cumulative release of about 68.8% in the same timeframe. A more pronounced effect was observed with the PEG-spacer conjugated formulations. The release from SLNP1FA and SLNP4FA was significantly slower and more controlled. Crucially, the degree of release retardation correlated with the length of the PEG spacer, with SLNP4FA demonstrating the most sustained release behavior among all formulations.

Table 8. Rationale of conjugation for synthesis of nanoconjugates

Nanoconjugates	Conjugating groups	Conjugating agents
SLNFA	Amine group of SLN and carboxylic group of folate	EDC NHS
SLNP1FA SLNP4FA	Conjugation of carboxylic group of folate and hydroxyl group of PEGs (Mw 1000, and 4000), then hydroxyl group of synthesized nanointermediate conjugated with amine group of SLN	DCC DMAP CDI

This behavior can be attributed to the role of the surface layers as an additional diffusion barrier. The solid lipid matrix itself controls the primary release rate, but the dense, hydrated corona formed by the FA and, more substantially, the PEG chains on the surface creates a more tortuous path for the drug to diffuse from the core into the bulk medium. The longer and more entangled PEG 4000 chains in the SLNP4FA formulation form a thicker and more effective barrier, thus providing the highest degree of release control. This property is of significant in vivo relevance, as it would minimize premature drug leakage during circulation and ensure that a greater fraction of the therapeutic payload is delivered to and released within the tumor microenvironment.

Table 9: Important peaks of FT-IR spectrum and data analysis of SLNFA

Wave number (cm^{-1})	Interpretation
789.83	Aromatic C-H bend
1128.08	Ester unconjugated C=O stretching
3445.95	N-H stretching of primary amine and O-H stretching
1128.08	Ester unconjugated C=O stretching
2252.92	Alkynyl C-H and C=C stretching
1673.75	Aromatic C=C bending and stretching due to attachment of FA
1416.11	CH-NH-C(=O) amides bending
1261.26	Esters unconj. C=O and C-O stretching
819.83, 789.83	Aromatic C-H bending

Table 10: Important peaks of FT-IR spectrum and data analysis of SLNP4FA

Wave number (cm^{-1})	Interpretation
3434.11	N-H stretch of primary amine
2923.72, 2871.61	Carboxylic acid C=O and O-H stretch
1643.13, 1735.88	
1458.03	CH-NH-C(=O) amides bending
1298.69, 1250.31	Esters C-O stretching
1107.21	C-O stretch ether linkage strong
950.80, 845.69	Aromatic C-H bending

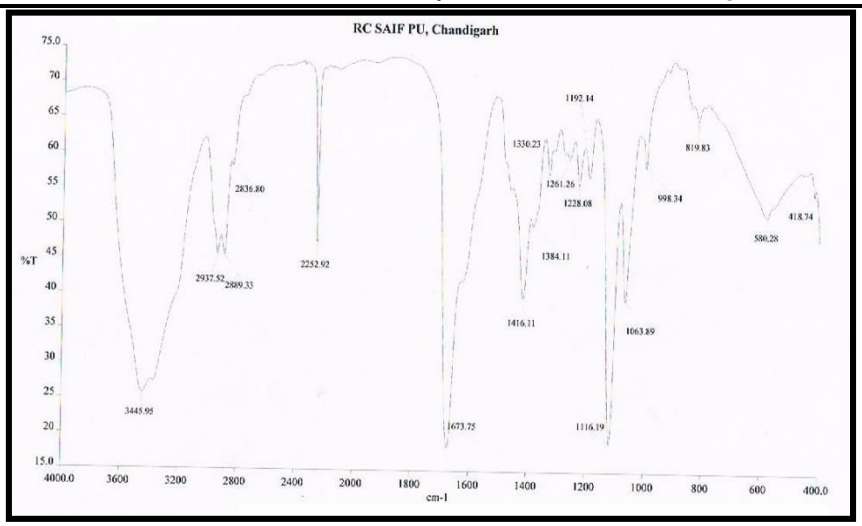

Figure 7: FT-IR spectrum of SLNFA

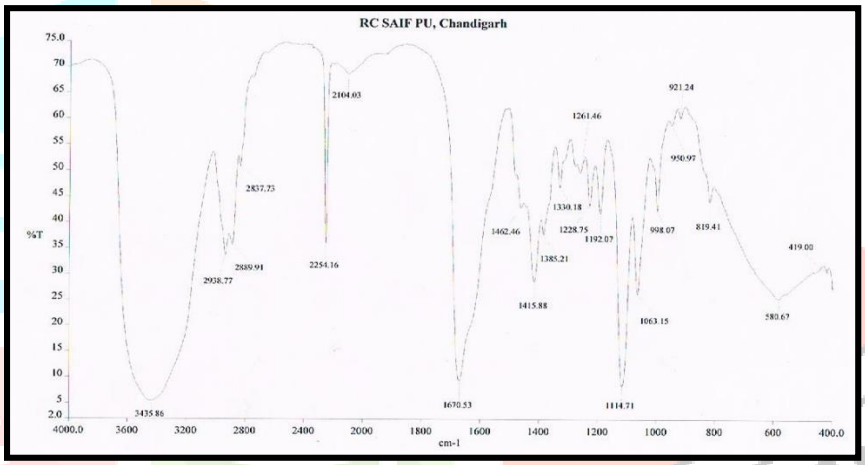

Figure 8: FT-IR spectrum of SLNP1FA

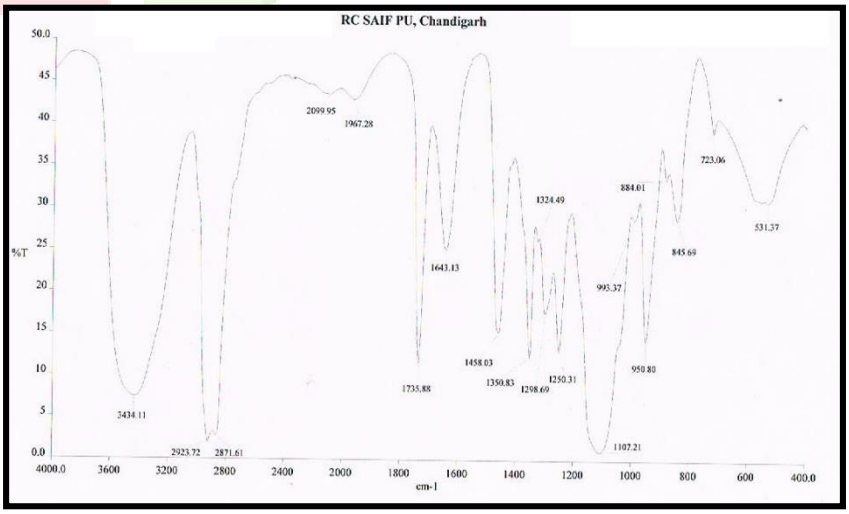

Figure 9: FT-IR spectrum of SLNP4FA

Table 11: ^{1}H NMR shifts and interpretation of the spectrum of SLNFA

δ value range (in ppm)	Integral values	Interpretation
1.0-2.0	0.9,1.3,1.5	R-(C=O0-NH-CH_2-CH_2-) methyl H-shift
2.0-2.9	2.5	Carbonyl
3.1-3.4	3.3	-CH_2NH_2 terminal group
6.0-8.5	6.6	Aromatic H- shift

Table 12: ^{1}H NMR shifts and interpretation of the spectrum of SLNP1FA

δ value range (in ppm)	Integral values	Interpretation
2.0-2.9	2.8	Carbonyl proton
3.0-3.4	3.3	Amide bond carbonyl proton
3.7-4.1	4.0	Ester bond proton
6-7	6.6	Aromatic proton
7.1-7.9	7.3	Amide bond nitrogen proton

Table 13: ^{1}H NMR shifts and interpretation of the spectrum of SLNP4FA

δ value range (in ppm)	Integral values	Interpretation
2.0-2.9	2.3	Carbonyl proton
3.0-3.4	3.2	Amide bond carbonyl proton
3.7-4.1	3.7	Ester bond proton
7.1-7.9	7.1	Amide bond nitrogen proton

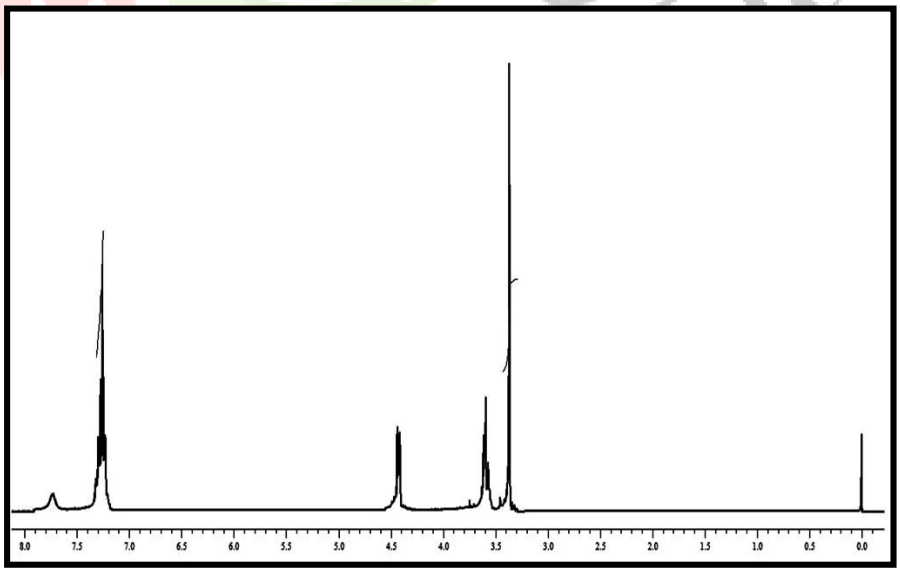

Figure 10: ^{1}H NMR spectrum of SLNFA

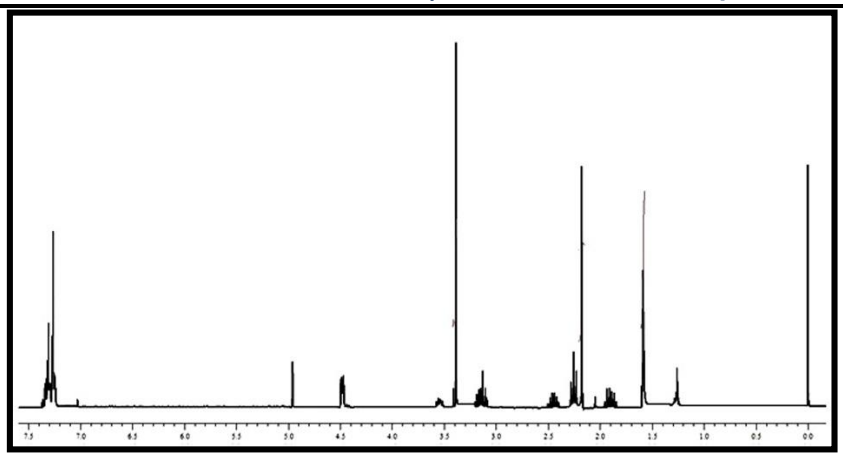

Figure 11: ^{1}H NMR spectrum of SLNP1FA

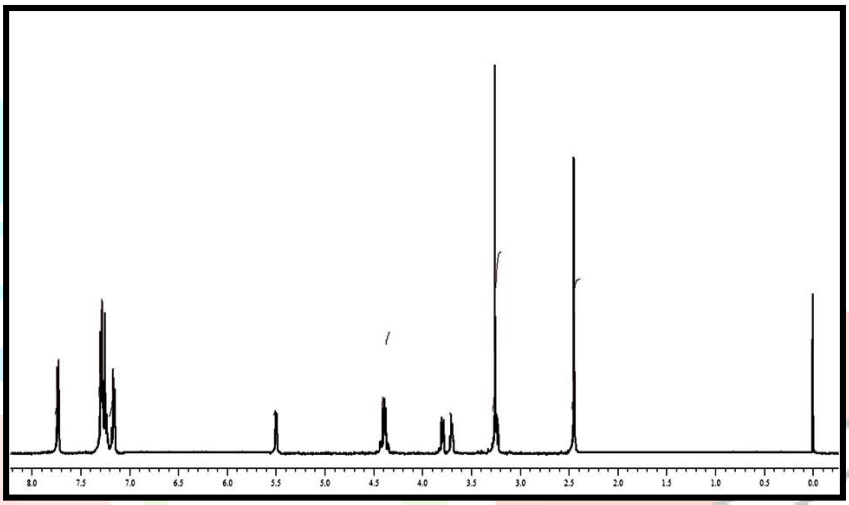

Figure 12: ^{1}H NMR spectrum of SLNP4FA

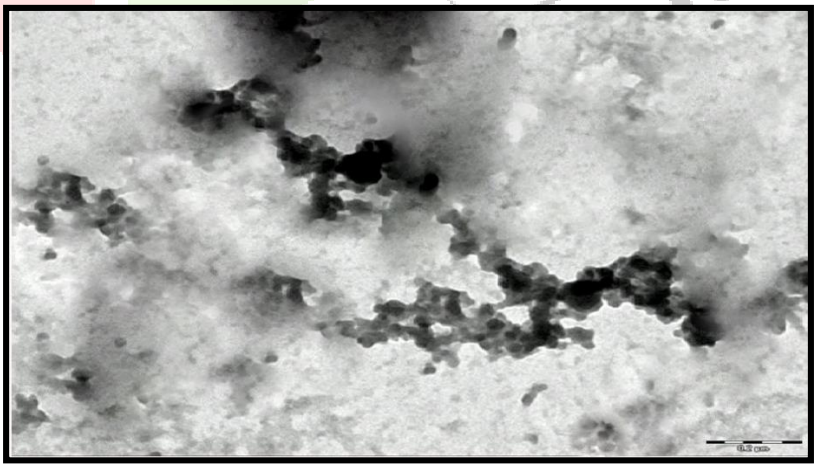

Figure 13: TEM photograph of SLNP4FA

3.4. Targeted Cytotoxicity against MCF-7 Cancer Cells

The ultimate test of the nanoformulations' design was their ability to effectively kill cancer cells. The in vitro cytotoxicity of free PTX and the various PTX-loaded nanoformulations was evaluated against the FR-positive MCF-7 human breast cancer cell line using the MTT assay after 48 hours of treatment. All formulations induced a dose-dependent decrease in cell viability. The calculated IC50 values, which represent the concentration required to inhibit 50% of cell growth, are presented in Table 2.

The results clearly demonstrate the therapeutic advantage conferred by the nanoparticle delivery system and the active targeting strategy. Free PTX exhibited an IC50 of 601.18 nM. Encapsulation in non-targeted plain SLNs resulted in a slightly lower IC50 of 567.45 nM, an effect likely attributable to improved cellular uptake of the nanoparticles compared to the free drug. However, the introduction of folate targeting led to a dramatic enhancement in cytotoxicity. The IC50 value for the directly conjugated SLNFA was 403.08 nM, significantly lower than that of the non-targeted controls. This confirms that the folate ligand successfully directs the nanoparticles to the MCF-7 cells, leading to enhanced intracellular drug delivery via FR-mediated endocytosis.

The central hypothesis of this study—that spacer length is a critical determinant of targeting efficiency—was unequivocally supported by the data. The PEG-spacer linked formulations were substantially more potent than the directly conjugated SLNFA. SLNP1FA (PEG 1000) achieved an IC50 of 370.34 nM, and SLNP4FA (PEG 4000) was the most effective formulation, with an IC50 of 331.29 nM. This establishes a clear hierarchy of potency: SLNP4FA > SLNP1FA > SLNFA > Plain SLN > Free PTX. The superior performance of the spacer-linked systems indicates that direct conjugation of FA to the SLN surface results in significant steric hindrance, which partially masks the ligand and impedes its ability to bind to the folate receptor. The flexible PEG spacer effectively overcomes this hindrance by extending the FA ligand away from the nanoparticle surface, making it more accessible for receptor binding. The fact that the longer PEG 4000 spacer in SLNP4FA conferred the greatest cytotoxic effect suggests that it provides the optimal length and flexibility to maximize this ligand-receptor interaction. The SLNP4FA formulation achieved a nearly 50% reduction in the required drug concentration to kill cancer cells compared to free PTX, a remarkable improvement in therapeutic efficacy driven by rational nanocarrier design.

Table 14: In Vitro Cytotoxicity of PTX-Loaded Nanoformulations against MCF-7 Cells after 48h Treatment.

Formulation	IC50 Value (nM ± SD)	% Reduction in IC50 (relative to Free PTX)
Free PTX	601.18 ± 18.22	0.00
Plain SLN	567.45 ± 15.26	5.61
SLNFA	403.08 ± 21.09	32.95
SLNP1FA	370.34 ± 10.91	38.40
SLNP4FA	331.29 ± 7.01	44.89

Data represent mean ± SD (n=3). IC50 values for PTX and SLN were calculated based on data from Table 8.1 in. The % Reduction in IC50 was calculated as * 100. The source provided a different set of IC50 values in Table 8.2; the values here are recalculated for consistency with the raw viability data presented.

3.5. Cellular Uptake and Targeting Specificity

To visually corroborate the quantitative cytotoxicity data, the morphological changes in MCF-7 cells after 48 hours of treatment were observed via microscopy. These studies provided qualitative evidence of the differential effects of the various formulations. Control (untreated) cells displayed a healthy, confluent monolayer morphology. Cells treated with free PTX and plain SLNs showed signs of cytotoxicity, including some cell rounding and a reduction in cell density, consistent with the MTT assay results. However, the effects were far more pronounced in the cells treated with the folate-targeted nanoparticles. Cells exposed to SLNFA, SLNP1FA, and especially SLNP4FA exhibited widespread cell death, characterized by significant cell rounding, detachment from the culture plate, and a drastically reduced cell population.

The enhanced cytotoxic morphology observed with the targeted formulations, particularly SLNP4FA, is a direct visual confirmation of their superior efficacy. This heightened effect is attributed to a more efficient cellular uptake process. The optimized presentation of the folic acid ligand on the SLNP4FA nanocarrier leads to a higher frequency of successful binding events with the folate receptors on the MCF-7 cell surface, triggering more efficient receptor-mediated endocytosis. This, in turn, results in a greater intracellular accumulation of the PTX payload, overwhelming the cancer cells' microtubule dynamics and leading to potent, targeted cell killing. These microscopic observations strongly support the conclusion drawn from the MTT assay: the superior cytotoxicity of the SLNP4FA formulation is a direct consequence of its optimized design, which maximizes the targeted delivery of paclitaxel into cancer cells.

4. Conclusion

This study successfully designed, synthesized, and characterized a series of folate-targeted, paclitaxel-loaded solid lipid nanoparticles to investigate the critical role of surface architecture in active tumor targeting. The work demonstrated that surface engineering with folic acid, both directly and via PEG spacers, is a viable strategy to create targeted nanocarriers. Spectroscopic and physicochemical analyses confirmed the successful synthesis of each distinct nano-architecture (SLNFA, SLNP1FA, and SLNP4FA).

The investigation yielded several key findings. First, surface functionalization with FA and PEG spacers significantly enhanced the drug entrapment efficiency of PTX, with the longest spacer (PEG 4000) yielding the highest payload. Second, these surface modifications created an additional diffusion barrier, resulting in a more controlled and sustained in vitro drug release profile, a highly desirable feature for in vivo applications.

The central conclusion of this research is that the length of the PEG spacer arm is a critical determinant of the biological efficacy of folate-targeted SLNs. Ex vivo cytotoxicity studies against FR-positive MCF-7 cancer cells revealed a clear structure-activity relationship. The formulation with the longest spacer, SLNP4FA (PEG 4000), exhibited markedly superior anti-tumor activity compared to the formulation with a shorter spacer (SLNP1FA), a directly conjugated ligand (SLNFA), and non-targeted controls. This enhanced efficacy is attributed to the ability of the long and flexible PEG 4000 spacer to optimally present the folic acid ligand for receptor interaction, thereby overcoming the steric hindrance imposed by the nanoparticle surface and maximizing the efficiency of receptor-mediated endocytosis.

In conclusion, this work provides compelling evidence that rational linker design is paramount in the development of effective actively targeted nanomedicines. By systematically optimizing the spacer length, it is possible to significantly enhance the therapeutic potential of the nanocarrier. The FA-PEG(4000)-SLN architecture identified in this study represents a highly promising and rationally designed platform for the targeted delivery of paclitaxel and other chemotherapeutic agents to solid tumors, offering a potential pathway to more effective and less toxic cancer treatments.

5. References

1. Bildstein L, Dubernet C, Couvreur P (2011) Prodrug-based intracellular delivery of anticancer agents. Adv Drug Deliv Rev 63, 3-23.

2. Boltri L, Canal T, Esposito PA, Carli F (1993) Lipid nanoparticles: Evaluation of some critical formulation parameters. Proc Intern Symp Control Rel Bioact Mater 20, 346-347.

3. Cavalli R, Caputo O, Gasco MR (2000) Preparation and characterization of solid lipid nanoparticle containing Paclitaxel. Eur J Pharma Sc 10, 305-309.

4. Chattopadhyay P, Shekunov BY, Yim D, Cipolla D, Boyd B, Farr S (2007) Production of solid lipid nanoparticle suspensions using supercritical fluid extraction of emulsions (SFEE) for pulmonary delivery using the AERx system. Adv Drug Deliv Rev 59, 444-453.

5. Chen H, Chang X, Du D, Liu W, Liu J, Weng T (2006) Podophyllotoxin-loaded solid lipid nanoparticles for epidermal targeting. J Control Release 110, 296-306.

6. Cortesi R, Esposito E, Luca G, Nastruzzi C (2000) Production of lipospheres as carriers for bioactive compounds. Biomaterials 23, 2283-2294.

7. Domb AJ (1993) United States Patent, US 5188837.

8. Ferrari M (2005) Cancer nanotechnology: opportunities and challenges. Nat Rev Cancer 5, 161-171.

9. Fry DW, White JC, Goldman ID (1978) Rapid separation of low molecular weight solutes from liposomes without dilution. J Anal Biochem 90, 809-815.

10. Gajbhiye V, Kumar PV, Tekade RK, Jain NK (2007) Pharmaceutical and biomedical potential of PEGylated dendrimers. Curr Pharma Design 13, 415-429.

11. Gajbhiye V, Kumar PV, Tekade RK, Jain NK (2009) PEGylated PPI dendritic architectures for sustained delivery of H2 receptor antagonist. E J Med Chem 44, 1155-1166.

12. Gasco MR (1993) Method for producing solid lipid microspheres having narrow size distribution. United States Patent, US 5188837.

13. Gasco MR (1997) Solid lipid nanospheres from warm microemulsions. Pharm Tech Eur 9, 52-58.

14. Gosselin PM, Thibert R, Preda M, McMullen JN (2003) Polymeric properties of micronized carbamazepine produced by RESS. Int J Pharm 252, 225-233.

15. Hayes ME, Drummond DC, Kirpotin DB (2006) Self-assembling nucleic acid-lipid nanoparticles suitable for targeted gene delivery. Gene Ther 13, 646-651.

16. Hu FQ, Zhang Y, Du YZ, Yuan H (2008) Nimodipine loaded lipid nanospheres prepared by solvent diffusion method in a drug saturated aqueous system. Int J Pharm 348, 146-152.

17. Indian Pharmacopoeia (1996, 2011). Govt of India, Ministry of Health and Family Welfare. New Delhi.

18. Jain NK (2001) Advances in Controlled and Novel Drug Delivery. CBS Publishers and Distributors, New Delhi, 1st ed. 40-69.

19. Jain RK, Stylianopoulos T (2010) Delivering nanomedicine to solid tumors. Nat Rev Clin Oncol 7, 653-664.

20. Jenning V, Gysler A, Schafer KM, Gohla S (2000) Vitamin A loaded solid lipid nanoparticles for topical use: Occlusive properties and drug targeting to the upper skin. Eur J Pharm Biopharm 49, 211-218.

21. Jenning V, Schafer-Korting M, Gohla S (2000) Vitamin A-loaded solid lipid nanoparticles for topical use: drug release properties. J Control Rel 66, 115-126.

22. Kateb B, Chiu K, Black KL, et al. (2011) Nanoplatforms for constructing new approaches to cancer treatment, imaging, and drug delivery: what should be the policy? Neuroimage 1, S106-124.

23. Kojima C, Kono K, Maruyama K, Takagishi T (2000) Synthesis of PAMAM dendrimers having PEG grafts and their ability to encapsulate anti-cancer drugs. Bioconj Chem 11, 910-917.

24. Kumar SS, Saha AK, Kavitha K, Basu SK (2012) Evaluation of clobazam loaded ionically cross-linked microspheres using chitosan. Der Pharmacia Sinica 3(6), 616-623.

25. Lan M, Zhu L, Wang Y (2020) Multifunctional nanobubbles carrying indocyanine green and paclitaxel for molecular imaging and the treatment of prostate cancer. J Nanobiotechnology 18, 121-125.

26. Leamon CP, Low PS (1994) Selective targeting of malignant cells with cytotoxin-folate conjugates. J Drug Target 2, 101-112.

27. Lee RJ, Low PS (1994) Delivery of liposomes into cultured KB cells via folate receptor- mediated endocytosis. J Biol Chem 269, 3198-3204.

28. Lee RJ, Wang S, Low PS (1996) Measurement of endosome pH following folate receptor-mediated endocytosis. Biochim Biophys Acta 1312, 237-242.

29. Lu B, Xiong SB, Yang H, Yin XD, Chao RB (2006) Solid lipid nanoparticles of mitoxantrone for local injection against breast cancer and its lymphnode metastases. Eur J Pharm Sci 28, 86-95.

30. Manjunath K, Suresh RJ, Venkateswarlu V (2005) Solid Lipid Nanoparticles as Drug Delivery Systems. Methods Find Exp Clinical Pharmacology 27, 120.

31. Martin A, Bustamante P, Chun AHC (1995) Physical Pharmacy. Waverly Pvt. Ltd., New Delhi, 4, 212, 404.

32. Moffat AC, Osselton MD, Widdop B (eds) (2005) Clarkes Analysis of Drugs and Poisons. 3rd edition, Pharmaceutical Press, USA.

33. Mosmann T (1983) Rapid colorimetric assay for cellular growth and survival: application to proliferation and cytotoxicity assays. J Immunol Meth 65, 55-63.

34. Muller et al. (1995) utilized SLNs as an alternative colloidal carrier system for controlled drug delivery and reported its various advantages over other carrier systems.

35. Neerman MF (2006) Enhancing the site specific targeting of macromolecular anti-cancer drug delivery system. Curr Drug Targets 7, 229-235.

36. Pandey R, Sharma S, Khuller GK (2005) Oral SLN Based antitubercular chemotherapy. Tuberculosis (Edinb) 85, 415-420.

37. Peer D, Karp JM, Hong S, Farokhzad OC, Margalit R, Langer R (2007) Nanocarriers as an emerging platform for cancer therapy. Nat Nanotechnol 2, 751-760.

38. Prashant Kesarwani, Rakesh K. Tekade, N. K. Jain (2011) Spectrophotometric estimation of paclitaxel. International Journal of Advances in Pharmaceutical Sciences 2, 29-32.

39. Quintana A, Raczka E, Piehler L, Lee I, Myc A, Majoros I, Patri AK, Thomas T, Mul J, Baker JR Jr (2002) Design and function of a dendrimer-based therapeutic nanodevice targeted to tumor cells through the folate receptor. Pharma Res 19, 1310-1316.

40. Ruckmani K, Sivakumar M, Ganeshkumar PA (2006) Methotrexate loaded solid lipid nanoparticles (SLN) for effective treatment of carcinoma. J Nanosci Nanotechnol 6, 2991-2995.

41. Santos MC, Mehnert W, Schaller M (2002) Drug targeting by solid lipid nanoparticles for dermal use. J Drug Target 10, 489-495.

42. Sashidharan KV, Rosaiah JN, Kumar A, Bid HK, Konwar R, Chattopadhyay N (2007) Cell growth inhibitory action of an unusual labdane diterpene, 13-epi-sclareol in breast and uterine cancers in vitro. Phytother Res 21, 1105-1108.

43. Shenoy VS, Vijay IK, Murthy RS (2005) Tumour targeting: Biological factors and formulation advances in injectable lipid nanoparticles. J Pharm Pharmacol 57, 411-422.

44. Sjostrom B, Bergenstahl (1992) Preparation of submicron drug particles in lecithin-stabilized o/w emulsions I. Model studies of the precipitation of cholestreryl acetate. Int J Pharm 88, 53-62.

45. Skehan P, Storeng R, Scudiero D, Monks A, McMahon J, Vistica D, Warren JT, Bokesch H, Kenney S, Boyd MR (1990) New colorimetric cytotoxicity assay for anticancer-drug screening. J Natl Cancer Inst 82, 1107-1112.

46. Soule HD, Vazguez J, Long A, Albert S, Brennan MJ (1973) A human cell line from a pleural effusion derived from a breast carcinoma. J Natl Cancer Inst 51, 1409-1416.

47. Tsuruo T, Naito M, Tomida A, Fujita N, Mashima T, Sakamoto H (2003) Molecular targeting therapy of cancer: drug resistance, apoptosis and survival signal. Cancer Sci 94, 15-21.

48. United States Pharmacopoeia-National Formulary (2007) The United States Pharmacopoeial Convention, USP 30th NF 25th edition.

49. Vasir JK, Labhasetwar V (2007) Biodegradable nanoparticles for cytosolic delivery of therapeutics. Adv Drug Deliv Rev 59, 718-728.

50. Wang LZ, Ho PC, Lee HS, Vaddi HK, Chan YW, Yung CS (2003) Quantitation of paclitaxel in micro-sample rat plasma by a sensitive reversed-phase HPLC assay. J Pharm Biomed Anal 31, 283-289.

51. Wang Y, Wu W (2006) In situ evading of phagocytic uptake of stealth solid lipid nanoparticles by mouse peritoneal macrophages. Drug Deliv 13, 189-192.

52. Westesen K, Siekmann B, Koch MHJ (1993) Investigations on the physical state of lipid nanoparticles by synchrotron radiation X-ray diffraction. Int J Pharm 93, 189-199.

53. Wissing SA, Muller RH (2001) Solid lipid nanoparticles (SLN) a novel carrier for UV blockers. Pharmazie 56, 783-786.

54. Yang SC, Lu LF, Cai Y, Zhu JB, Liang BW, Yang CZ (1999) Body distribution in mice of intravenously injected camptothecin solid lipid nanoparticles and targeting effect on brain. J Control Release 59, 299-307.

55. Zange R, Li Y, Kissel T (1998) Biocompatibility testing of ABA copolymers consisting of poly (l-lactic-co-glycolic acid) A blocks attached to a central poly (ethylene oxide) B block under in vitro conditions using different L929 mouse fibroblast cell culture models. J Control Release 56, 249-258.